THE ASTROPHYSICAL JOURNAL, 551:357–366, 2001 April 10
© 2001. The American Astronomical Society. All rights reserved. Printed in U.S.A.

INFRARED PROPERTIES OF WEAK RADIO SOURCES IN THE ρ OPHIUCHI MOLECULAR CLOUD[1]

BRUCE A. WILKING
Department of Physics and Astronomy, University of Missouri-St. Louis, 8001 Natural Bridge Road, St. Louis, MO 63121; brucew@newton.umsl.edu
SYLVAIN BONTEMPS
Observatoire de Bordeaux, Floirac F-33270, France; bontemps@observ.u-bordeaux.fr
RICHARD E. SCHULER
Department of Physics and Astronomy, University of Missouri-St. Louis, 8001 Natural Bridge Road, St. Louis, MO 63121; schuler@newton.umsl.edu
THOMAS P. GREENE
NASA/Ames Research Center, M.S. 245-6 Moffett Field, CA 94035-1000; tgreene@mail.arc.nasa.gov
AND
PHILIPPE ANDRÉ
CEA, DSM, DAPNIA, Service d'Astrophysique, Centre d'Etudes de Saclay, F-91191 Gif-sur-Yvette, CEDEX, France; pandre@cea.fr
Received 2000 June 30; accepted 2000 November 29

ABSTRACT

We report mid-infrared ISOCAM observations for a sample of radio continuum sources in the ρ Ophiuchi molecular cloud core with unknown or poorly studied infrared counterparts. These data are combined with existing infrared photometry, including recently published ISOCAM data, for previously studied radio sources to investigate the evolutionary states of 35 radio-emitting young stars in the ρ Oph cloud core. About 50% of the radio stars are found to have class I, flat, or class II spectral energy distributions with near-infrared excesses arising from circumstellar disks. Their radio emission is most likely thermal emission from gas ionized by stellar winds. The remaining radio emitters are young stars with class III spectral energy distributions that lack infrared excesses and circumstellar disks. Their radio emission likely is nonthermal emission from magnetic surface activity. The lack of young stars with weak infrared excesses supports earlier suggestions that disk dissipation is rapid. Class III sources are twice as common as class II sources in this radio-selected sample in comparison with extinction-limited samples, which underscores the importance of radio surveys in obtaining a complete census of young stellar objects. The concentration of diskless class III objects in the high column-density molecular core, and their median age of 0.3 Myr derived from their positions in a Hertzsprung-Russell diagram, indicate they are contemporaries of class II objects which include the classical T Tauri stars. It appears that these class III objects have shorter disk survival times than class II objects in the cloud.

Subject headings: ISM: individual (ρ Ophiuchi Cloud) — radio continuum: stars — stars: pre–main-sequence

1. INTRODUCTION

Radio surveys of molecular clouds have been an effective way to identify young stellar objects (YSOs) free of the effects of obscuring dust. Using radio interferometers such as the Very Large Array (VLA), these surveys have provided accurate positional information for YSOs with a wide range of evolutionary states (see Montmerle et al. 1993, André 1996, and Anglada 1996 for reviews). Heavily obscured class I objects and classical T Tauri stars are often associated with thermal radio continuum emission from gas ionized by their stellar winds. Objects in the earliest phase of evolution are often too weak to be detected at near-infrared (NIR) wavelengths but display strong thermal radio emission. Radio continuum emission from an extremely energetic wind led to the discovery of the class 0 source VLA 1623.4−2418 in ρ Oph (e.g., André et al. 1990). At the other end of the evolutionary spectrum, radio surveys have been one the most successful ways to identify YSOs with little or no circumstellar dust through detection of nonthermal continuum emission arising from magnetic surface activity. This latter group includes the strongest and most highly variable radio sources among YSOs (e.g., Feigelson & Montmerle 1985).

The ρ Ophiuchi molecular cloud has been the target of several radio continuum surveys (e.g., André, Montmerle, & Feigelson 1987; Stine et al. 1988; Leous et al. 1991; Bontemps 1996). At a distance of only $\sim$150 pc (de Zeeuw et al. 1999), it is one of the closest star-forming regions that is giving rise to an embedded cluster (Vrba et al. 1975; Elias 1978; Wilking & Lada 1983). A VLBI study of the strongest radio emitters ($S_\nu > 1$ mJy) by André et al. (1992) established that most are nonthermal sources associated with YSOs lacking circumstellar disks. Moreover, they showed that many of the diskless objects are concentrated in the cloud core and may be younger than the dispersed population of T Tauri stars. The most sensitive radio surveys, conducted by Leous et al. (1991, LFAM) and Bontemps (1996), have revealed a population of weaker radio sources ($S_\nu < 1$ mJy) with a mix of thermal and nonthermal sources. LFAM covered a 330 square arcmin region at $\lambda = 6$ cm encompassing high-density molecular gas in cores A, E, and F (Loren, Wootten, & Wilking 1990). They discovered 35 sources at $\geq$5 times the map noise level plus eight possible sources at 3–5 times the local rms noise. In the former group, only 12 could be identified with YSOs observed pre-

[1] *Infrared Space Observatory* (*ISO*) is an ESA project with instruments funded by ESA member states (especially the PI countries: France, Germany, the Netherlands, and the United Kingdom) and with the participation of ISAS and NASA.

viously in infrared surveys. The Bontemps (1996) survey covered a 36 square arcmin region at $\lambda = 3.6$ cm centered on the high-density gas in core B2 (Loren & Wootten 1986). Only three of the seven sources in their survey were identified with YSOs.

Using ISOCAM, we have conducted a survey of 12 radio sources at 6.7 and 11.5 μm with previously unknown or poorly studied infrared counterparts. Our goals were not only to discover new YSO counterparts to these weak radio sources but also to establish their evolutionary states. Of particular interest was the discovery of new low-luminosity class 0 or class I objects. Mid-infrared wavelengths are most sensitive to the presence of emission from circumstellar dust that marks the class 0 through classical T Tauri phase of evolution. Our survey found only four YSOs associated with these radio sources, which led us to expand our study to include 31 radio sources in the ρ Oph cloud with well-studied infrared counterparts. Special emphasis was placed on examining the nature of the weaker radio sources ($S_\nu < 1$ mJy) for comparisons with the stronger sources investigated by André et al. (1992). Our main result is that half of this radio-selected sample comprises YSOs with no detectable circumstellar dust. Using a Hertzsprung-Russell diagram, we discuss the ages and masses of these diskless objects in relation to classical T Tauri stars in the high column-density molecular core.

2. OBSERVATIONS

2.1. *ISOCAM Observations and Analysis*

ISOCAM observations were made in 1997 August toward the positions of 12 weak radio sources identified in surveys of the ρ Oph cores A and E/F by LFAM and core B2 by Bontemps (1996, OPHB2). The sources selected had previously unknown or poorly studied infrared counterparts. A summary of the ISOCAM observations is presented in Table 1. Briefly, observations at both $\lambda = 6.7$ μm (LW2) and $\lambda = 11.5$ μm (LW10) were made toward the VLA positions of nine sources using a 3.″0 and 1.″5 pixel field of view, respectively. The $\lambda = 11.5$ μm observations used a 4×4 raster with two pixel steps to cover a $57'' \times 57''$ area. The wider field $\lambda = 6.7$ μm observations covered a $108'' \times 108''$ region using a 3×3 raster with two pixel steps that enabled the observation of three additional radio sources.

The data were reduced using the CAM Interactive Analysis package. Individual frames were dark-subtracted and then cosmic-ray hits were removed using the multiresolution median transform (Starck et al. 1999) and a 10 σ clipping threshold. The transient response of the array was corrected using the inversion method (Starck et al. 1999). After removing a secondary dark residual, a flat field was constructed by median-combining individual raster frames with sources masked. No corrections were made for possible field distortion. Final calibration was achieved using the prelaunch conversion factors of 1 mJy = 2.19 ADU gain^{-1} s^{-1} for $\lambda = 6.7$ μm and 1 mJy = 3.99 ADU gain^{-1} s^{-1} for $\lambda = 11.5$ μm.

Aperture photometry was performed on the calibrated data and is presented in Table 1. For most of the $\lambda = 6.7$ μm sources, an aperture radius of 4.″5 was used with an aperture correction factor of 1.40. For most of the $\lambda = 11.5$ μm sources, an aperture radius of 2.″25 was employed with an aperture correction factor of 2.1. For the multiple source WL 20, a 6.″0 aperture was used in both filters with an aperture correction factor of 1.25 at $\lambda = 6.7$ μm and 1.32 at $\lambda = 11.5$ μm. To estimate the background emission in the

TABLE 1

SUMMARY OF ISOCAM OBSERVATIONS

Radio Source[a]	Position (B1950.0)[b] 16^h, $-24°$	Filters[c]	IR Sources[d]	S_ν (6.7 μm) (err) (mJy)	S_ν (11.5 μm) (err) (mJy)
LFAM 8	2328.3-1222.1	LW2, LW10	SKS 1–19	17.2 (0.3)	4.3 (0.2)
LFAM 10	2329.9-1148.5	LW2	none	<1.9	...
LFAM 15	2340.9-1942.4	LW2, LW10	GY 101	21 (1.0)	4.4 (0.3)
	...	...	GY 103[e]	13 (1.0)	2.7 (0.3)
LFAM p4	2353.1-2016.6	LW2, LW10	GY 154	8.7 (0.4)	9.5 (0.3)
	...	...	VSSG 5	90 (1.5)	...
LFAM 19	2357.2-2009.9	LW2	none	<2.4	...
LFAM 22	2358.5-1921.2	LW2, LW10	none	<2.4	<1.3
LFAM 25	2400.3-3201.7	LW2, LW10	none	<3.0	<1.7
LFAM 30	2413.9-3204.9	LW2, LW10	WL 20[f]	236.4 (1.3)	627.7 (1.6)
	...	...	GY 245	83.3 (1.1)	...
LFAM 31	2415.0-3015.9	LW2, LW10	none	<1.9	<1.2
LFAM 32	2415.6-2938.3	LW2, LW10	none	<1.9	<1.2
OPHB2 S3.....	2418.9-1711.0	LW2, LW10	none	<2.3	<1.5
OPHB2 S4.....	2423.3-1728.0	LW2	none	<2.3	...

[a] Radio source name from Leous et al. (1991, LFAM) or Bontemps (1996, OPHB2).

[b] Object R.A. (minutes, seconds) and decl. (arcminutes, arcseconds) in B1950.0.

[c] LW2 filter has a central wavelength of 6.7 μm and LW10 has a central wavelength of 11.5 μm.

[d] The infrared source on the same line as the VLA source is coincident within observational uncertainties. Source names are from infrared studies by Strom, Kepner, & Strom Table 1 (1995, SKS), Greene & Young (1992, GY), Vrba et al. (1975, VSSG), or Wilking & Lada (1983, WL).

[e] GY 103 lies 6″ south of GY 101 and LFAM 15.

[f] WL 20 is a close triple system as first noted by Strom, Kepner, & Strom (1995). At $\lambda = 2.2$ μm, the strongest components are separated east-west by $\sim 3.3''$. Ressler & Barsony (2001) have shown that beyond $\lambda = 7$ μm, the system is dominated by WL 20S. The ISOCAM source is highly variable at 6.7 μm and slightly extended at 11.5 μm. A 6″ aperture was used to measure the flux density. The positions of the NIR sources are not known accurately enough to establish which source is coincident with LFAM 30.

aperture, a sky annulus with a width of 6″–18″ placed well outside the aperture was used. The quoted uncertainty in the photometry is the composite rms noise calculated from the quadratic sum of (1) the rms of temporal fluctuations in the flux density of individual frames and (2) the rms in the background counts in the sky annulus. The uncertainties in the flux densities are dominated by the latter. Upper limits are 3 times the composite rms noise measured for two dummy apertures near the center of the field. The 1 σ sensitivity of our observations is estimated to be 0.8 mJy for $\lambda = 6.7$ μm and 0.4 mJy for $\lambda = 11.5$ μm.

The resulting photometry in the $\lambda = 6.7$ μm filter agrees with that obtained by the Nordh survey with an identical pixel field of view to within the mutual uncertainties in the flux densities (Abergel et al. 1996; Bontemps et al. 2001). A notable exception is WL 20, for which the flux density at 6.7 μm has increased from 161 mJy in 1996 (Bontemps et al. 2001) to 236 mJy in 1997 (this study) to 289 mJy in 1998 February (S. Bontemps, unpublished data).

3. RESULTS

3.1. *The Nature of Radio Sources in the ISOCAM Sample*

Table 1 shows that only four of the radio sources observed have associated infrared sources. All of these sources had been observed by prior NIR surveys. The LFAM 15 field contains the infrared sources GY 101 = ROC 16 and GY 103. With a separation of 6″, they are well resolved in both the 6.7 and 11.5 μm images. The position of LFAM 15 clearly associates the radio emission with GY 101. The LFAM 30 field contains the triple infrared source WL 20 (Strom, Kepner, & Strom 1995; Ressler & Barsony 2001). At $\lambda = 2.2$ μm, the strongest components are separated by $\sim 3''$ east-west with a weaker source $\sim 2''$ south of WL 20W. In our 6.7 μm image, the sources appear marginally resolved, with the two northern sources dominating the emission. The 11.5 μm image shows a single strong source with a weak extension to the northeast. This suggests that WL 20S dominates the emission at $\lambda = 11.5$ μm with the extension because of weaker emission by WL 20E. This structure is consistent with the images of Ressler & Barsony (2001). Astrometric data obtained by Ressler & Barsony (2001) identify the radio emission from LFAM 30 with WL 20S. A possible source was observed at 6.7 μm at the 2.5 σ level of 1.9 mJy in the LFAM 22 field. The position of R.A. (1950) = $16^{h}23^{m}59^{s}.7$, decl. (1950) = $-24°20'10''$ is well displaced from the VLA position for LFAM 22 and corresponds to no known NIR source to a limit of $K < 14$ mag (Barsony et al. 1997).

With the exception of the possible source in the LFAM 22 field, our observations revealed no new infrared sources. Our sensitivity to YSOs in the $\lambda = 6.7$ μm band can be estimated by assuming we can detect most objects that are ≥ 3 times our 1 σ sensitivity limit (Bontemps et al. 2001). For an object with no infrared excess, we have detected the majority of YSOs with $M \geq 0.08\ M_{\odot}$ at 1 Myr, which are obscured by as much as 40 mag of visual extinction.

We conclude that the eight radio sources in Table 1 not detected by ISOCAM are likely extragalactic in origin. These objects have neither NIR counterparts nor compact $\lambda = 1.3$ mm continuum emission (Motte, André, & Neri 1998). This includes the strong radio sources LFAM 19 and LFAM 22. The number of radio sources not identified with YSOs in the LFAM sample is 19 and consistent with the number of extragalactic radio sources estimated by LFAM for this field.

3.2. *A Comprehensive List of YSOs Associated with Radio Emission*

Our data were combined with that of radio sources previously identified with infrared or millimeter-wave counterparts in the L1688 main cloud to compile a list of all known radio continuum sources with stellar counterparts.[2] Our sample of 35 sources includes eight strong and 27 weak radio sources collected from the radio continuum surveys of André, Montmerle, & Feigelson (1987, ROC), Stine et al. (1988, SFAM), LFAM, André et al. (1992), André (1994 unpublished observations, A94a), and Bontemps (1996, OPHB2). Mid-infrared photometry from the Nordh survey in the $\lambda = 6.7$ μm (LW2) and $\lambda = 14.3$ μm (LW3) filters were used to supplement existing infrared data and define more clearly the spectral energy distributions for each radio star (Bontemps et al. 2001). These infrared sources are listed in Table 2 along with their radio and X-ray identifications.

3.3. *Spectral Energy Distributions for Radio-Emitting YSOs*

The shape of the spectral energy distribution (SED) from a YSO gives us clues to the amount and distribution of circumstellar dust and, hence, the evolutionary state (e.g., Lada 1987; André 1994). As it emerges from its cocoon of dust, the evolutionary state of a YSO can be characterized by the slope of the SED between near- and mid-infrared wavelengths. The slope, or spectral index, measures the quantity of warm circumstellar dust and is computed with the formula $a = d \log (\lambda F_{\lambda})/d \log \lambda$. Quantitatively, spectral indices greater than 0.3 describe class I SEDs from heavily obscured YSOs; such an SED is successfully modeled as a YSO surrounded by an optically thick disk and an infalling envelope (e.g., Adams, Lada, & Shu 1987). After stellar winds begin to dissipate this envelope, special viewing angles may give a relatively unobscured look at the photosphere/disk system. This yields a flat or double-peaked SED with a spectral index less than 0.3 but greater than -0.3. At a later time, only the star and optically thick disk remain, resulting in a class II SED characteristic of a classical T Tauri star (CTTS) and a spectral index between -0.3 and -1.6 (André & Montmerle 1994; Greene et al. 1994). Finally, as a YSO dissipates its circumstellar dust, the disk becomes optically thin, yielding a class III SED with a spectral index less than -1.6. These objects are classified with weak-lined T Tauri stars (WTTS), some of which are devoid of circumstellar material (e.g., the naked T Tauri stars; Walter et al. 1988).

For the infrared sources associated with radio emission, we computed the spectral index between the K band ($\lambda = 2.2$ μm) and the longest wavelength of observation between N ($\lambda = 10$ μm) and Q ($\lambda = 20$ μm). These spectral indices are presented in Table 2. Upper limits to spectral indices indicate that only a 3 σ upper limit was available for the long-wavelength flux density. Twenty-three of 35 sources have spectral types derived from spectroscopic observations; hence, their intrinsic colors and visual extinctions are known. GY 154, GY 289, and GY 101 have not been observed spectroscopically and were dereddened using NIR photometry and assuming $(H-K)_0 = 0.5$. Using these

[2] The only radio source with a YSO counterpart excluded from the list is ROX 39, which lies about 1° east of the cloud core.

TABLE 2

SPECTRAL INDICES AND SPECTRAL TYPES FOR RADIO EMITTERS

Optical/IR Source[a] (1)	Radio Source[b] (2)	X-Ray Source[c] (3)	Other[a] (4)	Spectral Type (5)	A_v (6)	Reference[d] (7)	Spectral Index[e] (8)	Dereddened Index[f] (9)	λ_{long} (μm) (10)	SED Class[g] (11)
	LFAM 5		VLA 1623.4-2418	...	...	...	...	...	...	0 (1)
WL 22	LFAM 23		IRS 27	...	...	...	2.4	...	20	I? (2)
WL 20S	LFAM 30?	ROXR1–39?		...	...	...	2.1	...	11.5	I (3)
YLW 16A	LFAM 35	ROXR1–45?	IRS 44 = GY 269	K8	...	LR99	1.7	...	20	I
GY 197	LFAM 26			...	...	...	1.3	...	14.3	I
YLW 15	ROC24 = LFAM 33	ROXR1–43	IRS 43 = GY 265	...	...	...	1.1	...	20	I
	LFAM 1	ROXR1-22?		...	...	...	0.86	...	20	I (4)
EL 29	LFAM 27	ROXA-8	YLW 7 = GY 214	...	...	...	0.47	...	20	I
GY 256	A94a	ROXR1-C7?		...	...	...	0.11	...	10	Flat
VSSG 27	LFAM 9		GY 51	M	22	GM95	0.33	−0.45	12.5	II (5)
				K3–M1	...	LR99				
GY 21	LFAM 3			M0	16	GL97	0.06	−0.53	10	II
				M0	14	LR99				
VSSG 17	OPHB2 S6		EL 33 = GY 279	>M2	28	GL97	0.05	−0.65	20	II
				K8	24	LR99				
VSSG 18	OPHB2 S5		EL 32 = GY 273	K6.5	18	LR99	−0.32	−0.96	10	II
GY 314	LFAM p8	ROXs27		M	4.9	GM95	−0.83	−1.0	10	II
				M0	7.1	LR99				
GSS 39	LFAM p3		EL 27 = GY 116	M	14	GM95	−0.49	−1.1	12.5	II
				K8	17	LR99				
GSS 29	LFAM p1	ROXs11	EL 18	K7–M0	12	GM95	−0.77	−1.2	10	II
				K6	11	LR99				
VSSG 4.....	LFAM p2		GY 81	K8	16	LR99	−0.60	−1.3	14.3	II
GY 154	LFAM p4			...	25:	est.	−0.56	−1.6	11.5	II
GY 232	LFAM p5			M0 III	...	LR99	−1.7	...	14.3	III (6)
GY 289	LFAM p7			...	23:	est.	−1.3	−2.2	14.3	III
GY 101	ROC16 = LFAM 15			...	50:	est	−1.2	−2.3	11.5	III
GSS 23	ROC8	ROXs8	DoAr 21 = EL 14	K1	5.7	LR99	−2.1	−2.3	10	IIID
				K0	6.6	BA92				
VSSG 22	ROC21	ROXs23		K7–M0	16	GM95	−2.2	−2.8	14.3	III
				K6	16	LR99				
WL 5	ROC20	ROXs22	IRS 38 = GY 246	F7	51	GM95	−0.97	−2.8	10	III
VSSG 14	ROC31	ROXR1-53	EL 36 = GY 372	A7	10	GM95	−2.4	−2.9	12.5	III
VSSG 11	ROC17	ROXC9	IRS 19	M3	14	GM95	−2.3	−2.9	14.3	III
				M0	14	LR99				
SKS 1–19	LFAM 8			M1.5	23	LR99	−2.0	−2.9	11.5	III
Source 1.....	ROC15 = LFAM 11	ROXs14	GSS 35 = EL 25	B4	10	BA92	−2.0	−3.1	4.8	IIID
GY 31	A94a			M5.5	56	WGM99	<0.5	<−1.6	10	III
GY 410	A94a			K7	9.6	LR99	<−1.7	<−2.1	10	III
				M6	10	GM95				
GY 253	A94a	ROXA-C7		M3	29	LR99	<−1.0	<−2.1	10	III
SR 12	LFAM p6	ROXs21		M0	0.7	LR99	<−2.1	<−2.1	10	III
				K4/M2.5	1.7	BA92				
ROX 31	ROC32	ROXs31	IRS 55 = GY 380	K7	4.3	BA92	<−2.3	<−2.5	10	III
VSSG 3.....	LFAM 18	ROXs17	GY 135	K7–M0	18	GM95	<−2.1	<−2.7	10	III
				K6	16	LR99				
GSS 30-IRS 2...	LFAM 2	ROXRA17	GY 12	M2	23	GM95	<−2.1	<−2.9	10	III
				K8	16	LR99				

[a] Source names are from optical or infrared studies by Struve & Rudkjobing (1949, SR); Grasdalen, Strom, & Strom (1973, GSS, Source 1); Vrba et al. (1975, VSSG,); Elias (1978, EL); Wilking & Lada (1983, WL); Montmerle et al. (1983, ROX); Castelaz et al. (1985, GSS 30-IRS 2); Wilking, Lada, & Young (1989, IRS); Young, Lada, & Wilking (1986, YLW); André et al. (1990, VLA); Greene & Young (1992, GY); Strom, Kepner, & Strom (1995, SKS, Table 1).

[b] Radio continuum sources are from André, Montmerle, & Feigelson (1987, ROC); Leous et al. (1991, LFAM); André (1994, unpublished observations, A94a); Bontemps (1996, OPHB2).

[c] X-ray source associations are from the *Einstein* survey by Montmerle et al. (1983, ROX), the *ROSAT* survey by Casanova et al. (1995, ROXR1), and Grosso et al. (2000, ROXRA), or the *ASCA* survey by Kamata et al. (1997, ROXA)

[d] References for spectral types and visual extinctions: Greene & Meyer (1995, GM95); Luhman & Rieke (1999, LR99); Bouvier & Appenzeller (1992, BA92); Wilking, Greene, & Meyer (1999, WGM99); Greene & Lada (1997, GL97). "est" indicates that A_v was estimated assuming $(H-K)_0 = 0.5$.

[e] Spectral index of the vF_v energy distribution from $\lambda = 2.2$ μm to the λ_{long} given in column 10.

[f] Spectral index computed after dereddening by amount shown in column 6.

[g] Spectral energy distribution class. "D" denotes a double-peaked SED. Individual notes include (1) VLA 1623 is a double source at $\lambda = 2.7$ mm separated by 1.″1 (Looney, Mundy, & Welch 2000), which coincides with two radio continuum sources (Bontemps & André 1997); (2) WL 22 has weak 1.3 mm emission and may be an obscured class II source (Motte et al. 1998); (3) WL 20S is the most luminous component in LW10 (see text); (4) LFAM 1 is a possible class 0 source (Motte et al. 1998); (5) VSSG 27 is a double source at 2.2 μm separated by 1.″15 (SKS); (6) GY 232 is classified as background giant by LR99.

values of A_v (see Table 2), infrared photometry from each source was dereddened using the extinction law of Rieke & Lebofsky (1985). For the ISOCAM bands and the Q band, we used the model of Draine & Lee (1984) to extrapolate the Rieke & Lebofsky law over these wavelengths. An independent analysis of the reddening in the $\lambda = 6.7$ and $\lambda = 14.3$ μm bands compared to the NIR confirms the value of A_λ/A_v obtained through this extrapolation to 14.3 μm but indicates a larger value at $\lambda = 6.7$ μm than the models suggest (Bontemps et al. 2001; Lutz et al. 1996). The resulting values for A_λ/A_v adopted by this study are 0.03, 0.05, 0.03, and 0.025 for $\lambda = 6.7$, 11.5, 14.3 μm, and Q, respectively. The spectral indices computed from the dereddened data are presented in Table 2.

As a check on how well the spectral indices reflected the long-wavelength slope of the SED, we plotted SEDs from $\lambda = 0.36$ μm to $\lambda = 20$ μm utilizing our data and photometry from literature when available. The primary sources for these data were Bouvier & Appenzeller (1992) for the optical data, Barsony et al. (1997) for the NIR data, and Greene et al. (1994) and Bontemps et al. (2001) for the mid-infrared data. Data from the *Infrared Astronomical Satellite* was not used because of confusion in these lower resolution data. While the plots are not shown here, the spectral indices computed from dereddened data do an excellent job in describing the overall SED shape. Foreground extinction may affect the SED classification of WL 22, which, despite its large spectral index, has weak $\lambda = 1.3$ mm emission (Motte et al. 1998). The classifications of YLW 15 (IRS 43), YLW 16a (IRS 44), and EL 29 as class I objects are consistent with their heavy-veiled infrared spectra (Greene & Lada 1996; Luhman & Rieke 1999; Greene & Lada 2000).

3.3.1. *Distribution of Spectral Indices*

The distribution of dereddened spectral indices is shown in Figure 1. Omitted from the sample are the class 0 and class I sources and the suspected field star GY 232.[3] The majority of spectral indices are computed from $\lambda = 2.2$–10 μm. Seven objects with upper limits to their spectral indices (mostly class III) are included. The distribution shows broad groupings around spectral indices of -1 and -2.5. The two groups appear distinct, as only two objects have a between -1.3 and -2.1 and one of these values is an upper limit. This gap in spectral indices is seen in unbiased surveys of star-forming regions and most likely signals a rapid evolution from a CTTS to class III phase (e.g., Bontemps et al. 2001). Yet this bimodal distribution also emphasizes a division based on the mechanism for the radio emission, with stellar winds generating the radio emission for the class I/II sources (dereddened $a > -1.3$) and magnetic surface activity for the class III sources (dereddened $a < -2.1$). Such a division is well established for sources with well-studied radio properties. Nonthermal radio emission from YSOs with class III SEDs has been identified through flarelike variability, circularly polarized emission, and high brightness temperatures in compact regions (<5 mas). In ρ Oph, these sources include GSS 23 = DoAr 21 (Feigelson & Montmerle 1985), ROX 31 (SFAM), and VSSG 14, Source 1, WL 5, GY 101 = ROC 16, and VSSG 11 (André et al. 1992). Thermal radio emission associated with stellar winds has been identified with class 0/I sources through radio structures extended on a scale of $\sim 1''$ (e.g., Anglada 1996). A prime example in ρ Oph is the class I source YLW 15, the strong radio emission of which was resolved out by VLBI observations (André et al. 1992). The mechanism for the radio emission is less clear for CTTS and could be nonthermal in sources with weak disk signatures (see § 3.3.3).

[3] The source GY 232 is classified as M0 III by Luhman & Rieke (1999). It is offset 5″ east from the VLA position of LFAM p5 and is probably unrelated to the radio emission observed by LFAM.

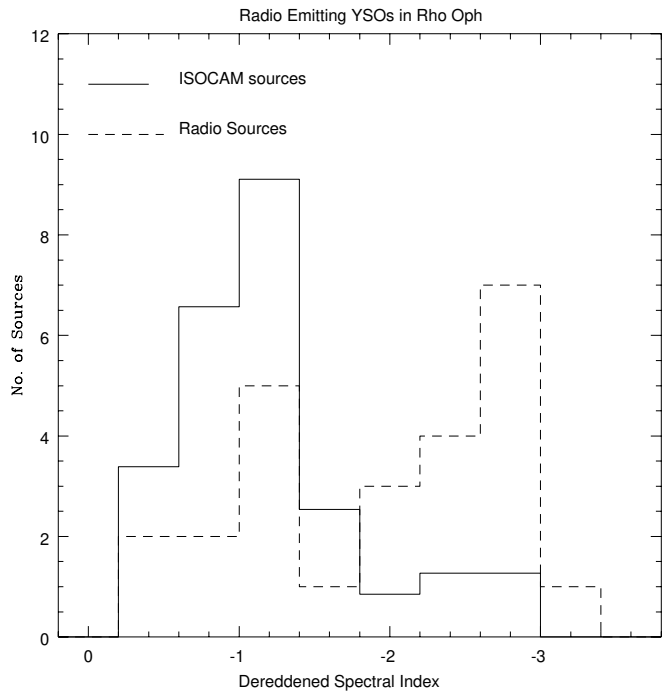

FIG. 1.—Distribution of dereddened spectral indices for 25 radio-emitting young stars (*dashed line*) and for 118 young stars identified in the ISOCAM survey of the ρ Oph cloud by Bontemps et al. (2001) (*solid line*). Included in the radio-emitting sample are seven objects with only upper limits to their spectral indices. The ISOCAM sample has been normalized to the total number of sources in the radio sample.

For comparison, also shown in Figure 1 is the distribution of dereddened spectral indices for $\lambda = 2.2$–14.3 μm for 118 young objects observed in the ISOCAM survey of the ρ Oph cloud (Bontemps et al. 2001) and normalized to the total number in the radio source histogram. The distribution of spectral indices is similar for both samples with the exception of a relatively higher fraction of class III objects in the radio source sample. This reflects the enhanced sensitivity that radio surveys have to class III objects relative to mid-infrared surveys that are most sensitive to sources with an infrared excess.

3.3.2. *Evolutionary States of Radio Emitters*

SED classes based on the spectral indices (dereddened when available) are presented in Table 2. Our analysis suggests that the radio-emitting objects are made up of 1 class 0 SED, 8 class I/flat, 9 class II, and 16 class III objects. These classifications are consistent with those derived from the bolometric temperature of each SED (Myers & Ladd 1993; Chen et al. 1995) and from the mass and distribution of circumstellar material derived from millimeter-continuum observations (André & Montmerle 1994; Motte et al. 1998). Objects with little or no circumstellar dust make up about half of the radio sample, and they are twice as common as class II sources. It appears that radio surveys are biased toward the detection of class III sources since the ratio of

class II to class III sources in extinction-limited samples from the ρ Oph core is close to 1:1.[4] It has been suggested that radio surveys are less sensitive to class II sources because of free-free absorption of nonthermal emission from the stellar surface by partially ionized outflows (André 1996). Radio surveys are an essential component of a complete census of a YSO population. Infrared surveys are incomplete for objects with class III SEDs since such objects appear indistinguishable from background stars, and X-ray surveys miss some class III objects when visual extinctions are high.

As noted by previous studies, the strongest radio emitters in the ρ Oph cloud have class III SEDs (André et al. 1987; Stine et al. 1988). Ten objects in our sample have $S(6\ \mathrm{cm}) > 1$ mJy and include Source 1, GY 101 = ROC 16, GSS 23, VSSG 11, WL 5, VSSG 22, ROX 31, VSSG 14, and YLW 15. Of these, only YLW 15 does not have a class III SED (it is class I). Among weaker radio sources, the evolutionary types are mixed with nearly equal numbers of class I/flat, class II, and class III objects. Only $\sim$30% of the weaker radio sources have class III SEDs.

3.3.3. *Disk Properties of the Radio Emitters*

Using a color-color diagram, the excess emission arising from the inner regions ($\leq$1 AU) of a circumstellar disk can be observed. A $(J-H)$ versus $(H-K)$ diagram is shown in Figure 2 for 23 YSOs associated with radio emission. Reddening lines are shown relative to the locus of main-sequence dwarfs and CTTS (Meyer, Calvet, & Hillenbrand 1997). In general, sources fall in the diagram as predicted by their SEDs, considering their $\pm 1\ \sigma$ errors: class III objects with little or no disk emission are found within the reddening band for dwarfs stars and class II sources with stronger disk signatures are found within the reddening band for CTTS (e.g., Lada & Adams 1992). Notable exceptions include GSS 30-IRS 2 (GY 12), which has a class III SED but lies to the right of the dwarf reddening band, and WL 20S, which has a class I SED but no K excess. For GSS 30-IRS 2, it is possible that the NIR reflection nebula associated with GSS 30-IRS 1 contributes to its apparent excess at K. Because of the extended nature of WL 20S (Ressler & Barsony 2001), it is possible that the NIR colors have contributions from scattered light that distort its position in the color-color diagram (Kenyon et al. 1993).

The excess emission at $\lambda = 2.2\ \mu$m caused by circumstellar dust can be measured quantitatively either by assessing the veiling in the K-band spectra or by comparing broadband colors to the intrinsic colors determined spectroscopically. In Table 3, we show values calculated for the infrared excess using broadband colors for sources of known spectral type. Sources with class III SEDs were dereddened to intrinsic dwarf colors and $r_k = F_{K\mathrm{ex}}/F_k$ was computed assuming $r_j = r_h = 0$. Hence, these values of r_k are lower limits. Class II sources within the CTTS reddening band were dereddened to the CTTS locus, and r_h and r_k were computed using the appropriate intrinsic dwarf colors and assuming $r_j = 0$. For comparison with the study of T Tauri stars by Skrutskie et al. (1990), we also have computed the infrared excess at $\lambda = 2.2$ and 10 μm in logarithmic units. In the last column of Table 3, we present values for r_k determined spectroscopically. These values generally agree with those derived from broadband colors given the typical uncertainties of 0.25–0.5. Poor agreement for VSSG 17 and VSSG 18 may be caused by variability in the veiling observed for the CTTS phase (e.g., Luhman & Rieke 1999).

Table 3 shows that radio-emitting YSOs with class III SEDs have optically thin inner disks ($\Delta K < 0.2$ and $\Delta N < 1.2$). This is consistent with the idea that the inner disk has been depleted through accretion, stellar winds, and/or the formation of planets and that the radio emission arises from magnetic surface activity. One would expect that the majority of radio-emitting YSOs with class II SEDs have optically thick inner disks if they are actively accreting. This appears to be the case for GY 21, VSSG 17, VSSG 18, and VSSG 4. However, we note that three of the class II

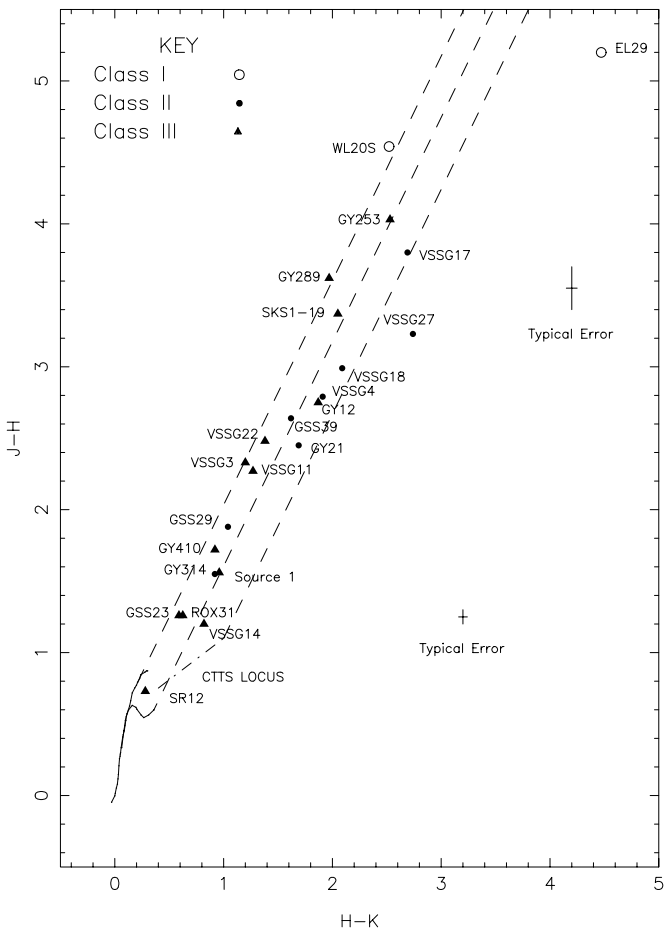

FIG. 2.—Color-color diagram for 23 of the 36 radio sources. All data and intrinsic colors are in the CIT system. JHK photometry was adopted from Barsony et al. (1997), except for WL 20S, for which data by Ressler & Barsony (2001) obtained with ProtoCam and transformed into the CIT system were used. Intrinsic dwarf and giant colors (*solid lines*) were adopted from Tokunaga (2000) and transformed into the CIT system using the conversions of Bessell & Brett (1988). The CTTS locus (*dash-dotted line*) is that determined by Meyer et al. (1997). The reddening lines (*dashed lines*) bands represent the slope of $(J-H)/(H-K) = 1.57$ found by Kenyon, Lada, & Barsony (1998). Typical uncertainties of $\pm 1\ \sigma$ as adopted from the Barsony et al. (1997) data are shown for both fainter sources (*top*) and brighter sources (*bottom*). The uncertainty in the J measurement of WL 20S is estimated to be $\pm$0.5 mag (M. E. Ressler 2000, private communication).

[4] Using the ρ Oph sources observed spectroscopically by Luhman & Rieke (1999), the ratio of class II to class III objects is 21 to 19 in a sample with $A_v < 21$ mag and $M > 0.1\ M_\odot$ for an age of 0.3 Myr. For X-ray sources observed by Grosso et al. (2000) in a region of the ρ Oph cloud observed both by *ROSAT* and ISOCAM, the ratio of class II to class III objects is 13 to 11 for $A_v < 10$ mag and $L_* > 0.3\ L_\odot$.

TABLE 3

INFRARED EXCESSES FOR RADIO EMITTERS

Source	r_h[a]	r_k[b]	ΔK[c]	ΔN[d]	r_k (Sp)[e]
			Class II		
GY 21	0.32	1.4	0.37	2.0	$r_k = 1$ (GL97)
VSSG 17	0.58	2.6	0.56	2.1	$r_k = 1$ (GL97)
VSSG 18	0.52	2.2	0.51	1.8	$r_k = 0$ (LR99)
GY 314	0.13	0.47	0.17	1.4	$r_k = 0.5$ (LR99)
GSS 39	0.16	0.64	0.21	1.3	$r_k = 0.75$ (LR99)
GSS 29	0.06	0.25	0.10	1.3	$r_k = 0$ (LR99)
VSSG 4.....	0.43	1.8	0.44	...	$r_k = 1$–2 (LR99)
			Class III		
GSS 23	0.0	0.14	0.06	0.45	$r_k = 0$ (LR99)
VSSG 22	0.0	0.13	0.05	...	$r_k = 0$ (LR99)
VSSG 14	0.0	0.13	0.05	0.12	$r_k = 0$ (LR99)
VSSG 11	0.0	0.02	0.01	<0.8	$r_k = 0$ (LR99)
SKS 1–19.....	0.0	0.36	0.13	...	$r_k = 0$ (LR99)
Source 1	0.0	0.06	0.03	...	$r_k = 0$ (LR99)
GY 410	0.0	0.17	0.07	<0.5	$r_k = 0$ (LR99)
GY 253	0.0	0.25	0.10	<0.6	$r_k = 0$ (LR99)
SR 12	0.0	0.06	0.03	<0.5	$r_k = 0$ (LR99)
ROX 31	0.0	0.08	0.03	<0.2	...
VSSG 3.....	0.0	0.04	0.02	<0.2	$r_k = 0$ (LR99)
GY 12	0.0	0.40	0.15	<0.4	$r_k = 0$ (LR99)

[a] $r_h = F_{Hex}/F_H = (10^{[(J-H)-(J-H)_0-0.11*A_v]/2.5} - 1)$ and assumes $r_j = 0$ and $A_v = 9.09\ E(J-H)$. $r_h \equiv 0$ for sources dereddened to intrinsic dwarf colors.

[b] $r_k = F_{Kex}/F_K = [(1 + r_h)(10^{[(H-K)-(H-K)_0-0.065*A_v]/2.5})] - 1$ where A_v is defined as above. $r_k > 0.58$ for an optically thick disk.

[c] $\Delta K = \log(1 + r_k)$ and is greater than 0.2 for an optically thick disk (Skrutskie et al. 1990).

[d] $\Delta N = (K + \Delta K*2.5 - N - 0.06*A_v)/2.5$ and assumes $(K-N)_0 = 0$. $\Delta N > 1.2$ for an optically thick disk (Skrutskie et al. 1990).

[e] Value determined spectroscopically by Luhman & Rieke (1999) or Greene & Lada (1997).

sources (GY 314, GSS 39, and GSS 29) have small K excesses ($\Delta K \leq 0.2$) and large N excesses ($\Delta N > 1.2$). It appears the innermost disks have been cleared, marking an end (at least temporarily) to accretion. Given the relationship between accretion and stellar winds (Bontemps et al. 1996), it is quite possible that the radio emission from these class II objects is nonthermal.

3.3.4. *Distribution of Radio Emitters*

The projected distribution of the 34 radio sources with associated YSOs is shown in Figure 3 in relation to contours of $C^{18}O$ column density and the locations of dense molecular cores. For reference, the boundaries of the LFAM and Bontemps (1996) surveys are also shown. It is remarkable that all objects are associated with the high column-density gas in the L1688 cloud in light of the fact we considered sources from the André et al. (1987) VLA survey, which covered an area 6.5 times larger than that shown in Figure 3. The concentration of class III sources in the molecular cloud was first noted by André et al. (1992) and remains significant in our larger sample. While the majority of radio sources associated with the dense molecular cores are in a class 0/I/II phase of evolution (see also Strom et al. 1995), class III sources are not excluded from these areas. About 30% of the radio sources detected in the deep radio surveys of the A, B, E, and F dense cores are class III objects, with the highest concentration in core A. Consistent with the idea that class III radio sources are embedded in

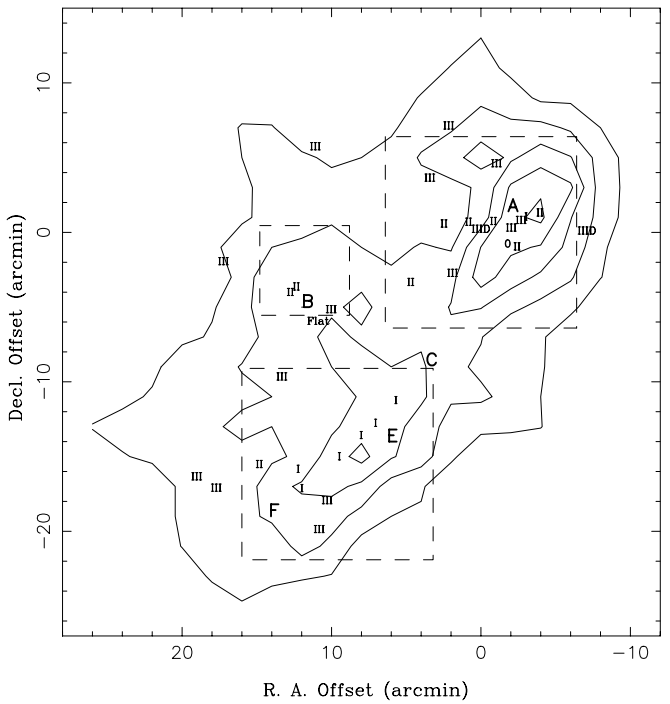

FIG. 3.—Distribution of 34 radio-emitting YSOs relative to high column-density $C^{18}O$ molecular gas. Excluded from the sample in Table 2 is the possible background giant GY 232. Solid lines are contours of $C^{18}O$ (2–1) integrated intensity, beginning at 2 K km s^{-1} and increasing in steps of 2 K km s^{-1} (Wilking 1991). Boldfaced letters A, B, C, E, and F mark the approximate locations of dense molecular cores as defined by $H^{13}CO^+$ or DCO^+ emission (Loren et al. 1990). The positions of the radio-emitting YSOs are labeled by their SED class: 0, I, flat, II, or III. The position of LFAM 1 has been artificially offset 10″ west and north of its true position to remove the coincidence of its plot symbol with that of GY 12. The (0, 0) position is the location of Source 1 (EL 25): $\alpha(2000) = 16^h26^m34^s.2$, $\delta(2000) = -24°23'27''$. Large dashed boxes show the boundaries of the LFAM VLA survey at $\lambda = 6$ cm and the small dashed box the $\lambda = 3.6$ cm survey by Bontemps (1996). We note that the boundaries of the southern survey by LFAM are misplotted in Fig. 1 of their 1991 paper. Most of the class III objects falling outside of these survey boxes were detected in the wider area survey by André et al. (1987) and include (*clockwise from bottom*) ROX 31, GY 410, VSSG 14, VSSG 22, VSSG 11, and GSS 23 = DoAr21.

the molecular gas is that they have the same median visual extinction ($A_v = 16$ mag) as the class II radio sources (see Fig. 2, Table 2).

3.4. *The Nature of Class III Radio Sources Associated with Dense Cores*

Are the class III sources that lie toward the high column-density gas (1) young objects embedded in the cloud with shorter than average disk survival times or (2) older pre–main-sequence (PMS) stars seen only in projection toward the cloud? Relative to isochrones in the models by D'Antona & Mazzitelli (1994, 1997), the median age of YSOs in the ρ Oph cloud core (including both class III objects and heavily veiled CTTS) is 0.3 Myr (Luhman & Rieke 1999). This is nearly identical to the age of 0.4 Myr derived from modeling the luminosity function of 118 class II sources observed in the ISOCAM survey of the ρ Oph cloud (Bontemps et al. 2001). Given an average disk survival timescale of 3×10^6 yr (Strom et al. 1989), one would expect that the majority of YSOs in the ρ Oph core would possess circumstellar disks. In the following section, a Hertzsprung-Russell diagram is used to discuss evidence

that the majority of the class III radio sources in ρ Oph are contemporaries of the previously studied YSO population but have shorter than average disk survival times.

3.4.1. *Location in the Hertzsprung-Russell Diagram*

Effective temperatures and stellar luminosities have been estimated for a subsample of the radio sources using spectral classifications by Greene & Meyer (1995), Luhman & Rieke (1999), and Wilking, Greene, & Meyer (1999) (see Table 2), and NIR photometry by Barsony et al. (1997). For most sources, intrinsic colors and visual extinctions were estimated using the $(J-H)$ versus $(H-K)$ diagram shown in Figure 2. Spectral types were converted to effective temperatures using the temperature scale presented by Tokunaga (2000). Because of the small $\lambda = 2.2$ μm excesses, absolute J magnitudes could be converted to stellar luminosities using data compiled by Tokunaga (2000) with infrared colors and bolometric corrections transformed to the CIT system using the conversions of Bessell & Brett (1988). Stellar luminosities for WL 5 and GY 31 were calculated using their $(H-K)$ colors and absolute K magnitudes. The bolometric luminosity for Source 1 was taken from Lada & Wilking (1984). No attempt was made to deredden strong excess sources VSSG 27 and EL 29 and they were eliminated from further consideration.

Figure 4 shows an H-R diagram for 21 radio sources with spectroscopic data relative to the theoretical tracks and isochrones of F. D'Antona & I. Mazzitelli (1997; 1998, private

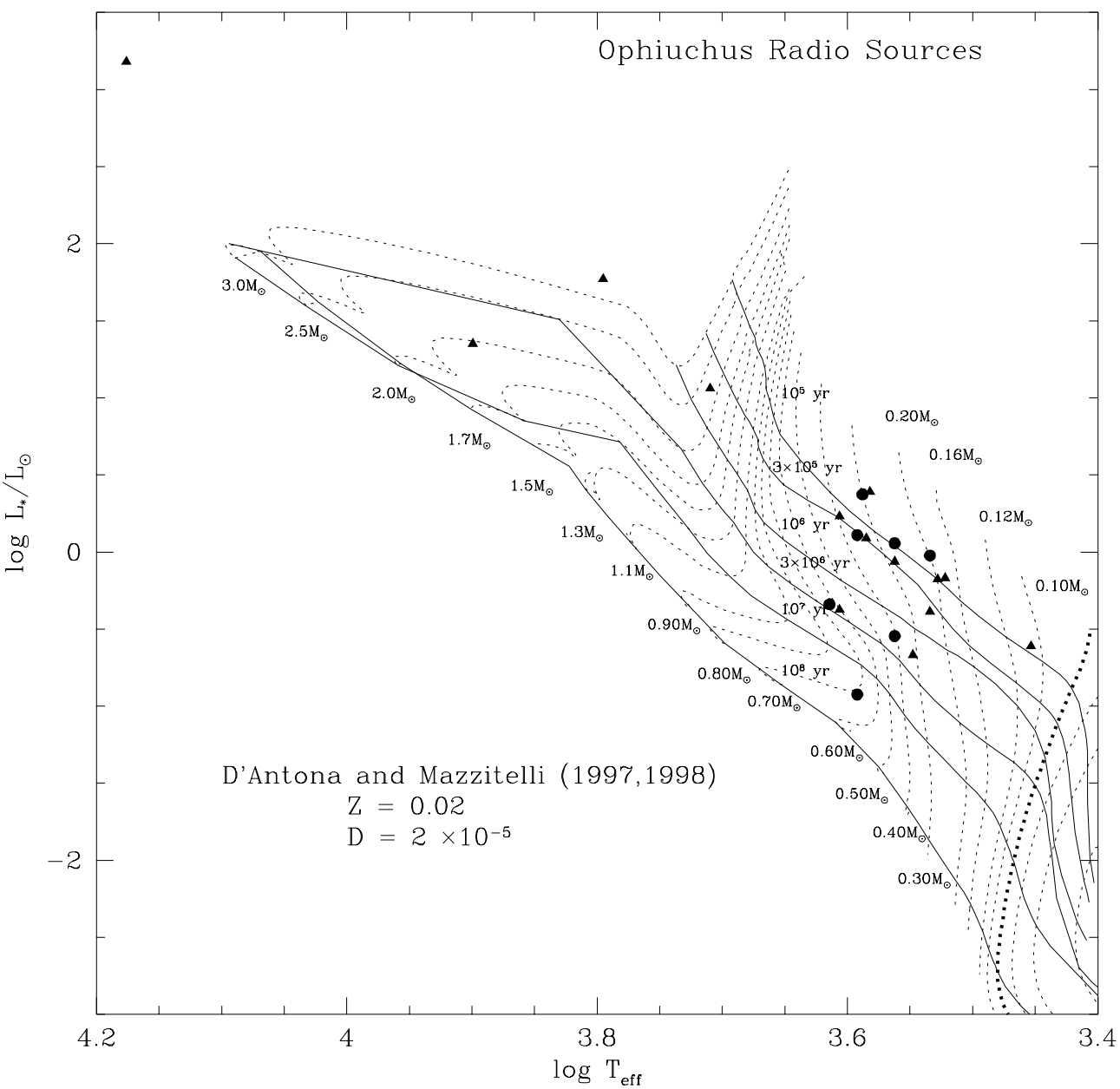

FIG. 4.—Hertzsprung-Russell diagram of the radio-emitting YSOs with spectroscopic observations. Theoretical tracks and isochrones are from F. D'Antona & I. Mazzitelli (1997; 1998, private communication). The boldfaced dashed line marks the hydrogen-burning limit. Filled triangles mark the locations of objects with class III SEDs that resemble reddened blackbodies. Filled circles mark the locations of objects with class II SEDs and significant infrared excesses. Effective temperatures of GSS 29 and VSSG 3, and VSSG 11 and GY 253, have been artificially offset by 0.0003 dex to distinguish more clearly their plot symbols.

communication) assuming $Z = 0.02$ and $D/H = 2 \times 10^{-5}$. Different plot symbols are used for objects with class II and class III SEDs. The four most massive stars in the radio-emitting sample—Source 1, VSSG 14, WL 5, and GSS 23—all have class III SEDs. The remaining sources have masses between 0.1 $M_\odot$ (GY 31) and 0.8 $M_\odot$ (VSSG 4) and range in age from less than 10^6 yr to 10^7 yr. The median age for the low-mass sample is 0.3 Myr, which is consistent with ages derived from the same models for the magnitude-limited spectroscopic sample of class II and III objects (Greene & Meyer 1995; Luhman & Rieke 1999) and from the luminosity function for class II sources identified by ISOCAM (Bontemps et al. 2001). These results are unchanged when using the PMS tracks and isochrones of Palla & Stahler (1999), which consider PMS initial conditions from the protostellar phase. Eight of the class III sources sit above the 1 Myr isochrone. They are (from warmest to coolest) ROX 31, VSSG 3, VSSG 22, SR 12, GY 12, VSSG 11, GY 253, and GY 31. We conclude that *the low-mass radio sources with class III SEDs are coeval with the general YSO population in the core.*

It is well known that among T Tauri stars there is a range of disk survival times. Studies of TTs in Taurus-Auriga find that for an age of ≤ 1 Myr, 12 of 23 objects have optically thin disks (see Table 2 in Skrutskie et al. 1990). In the LFAM survey box of core A, there are 23 YSOs in an extinction-limited sample ($K < 10$ to $K < 12$ for $A_v = 0$ to 20 mag). Using the SED classifications of Luhman & Rieke (1999), Wilking, Lada, & Young (1989), and this study, it is found that at least seven of 23 of the low-mass YSOs have class III SEDs, which implies little or no circumstellar dust. This is consistent with the fraction in Taurus-Auriga when one considers the small sample sizes and differences in the PMS models. The short disk-survival times observed for a fraction of the YSO population have been discussed in the literature. Walter et al. (1988), in their comparisons of "naked" T Tauri stars (NTTS) with CTTS, propose that NTTS are YSOs that have had the supply of gas to their accretion disks cut off by some mechanism that is yet to be identified but which could involve peculiar stellar velocities relative to the cloud, binary companions, or the formation of a circumstellar disks from material with lower specific angular momentum. André et al. (1992) suggest that a strong fossil field in the disk could accelerate accretion and deplete the inner disk.

4. SUMMARY

Using ISOCAM, a sample of radio sources found in VLA surveys of the ρ Oph cloud core with previously unknown, or poorly studied, infrared counterparts has been observed. YSO counterparts were identified for four of 12 radio sources, all previously observed NIR objects. No new cold class 0 or I sources were found associated with these radio sources and the majority appear to be extragalactic objects.

Using our survey and previously published data, the evolutionary states of 35 radio sources in ρ Oph with known infrared or millimeter wavelength counterparts has been investigated. About 50% of the radio sources are associated with young stars with class I, flat, or class II SEDs and optically thick disks. Their radio emission is most likely thermal emission from gas ionized by stellar winds that are characteristic of this phase of evolution. However, several class II sources that have dissipated much of their innermost disks and may be associated with nonthermal radio emission are identified. The other 50% are associated with YSOs with class III SEDs that appear as reddened blackbodies. The SEDs, the lack of NIR excesses, and the lack of millimeter-continuum emission suggests that these objects are truly diskless. As noted previously by André et al. (1992), the percentage of class III sources increases to 90% when considering only the strongest radio emitters. The radio emission from class III objects is likely nonthermal emission from magnetic surface activity. The scarcity of objects with weak infrared excesses confirms earlier suggestions that disk dissipation is rapid.

Using an H-R diagram, the masses and ages of the radio-emitting YSOs have been estimated. Among objects with masses ranging from 0.1 to 0.8 $M_\odot$ and associated with dense cores, 30% are class III objects. The median age of these diskless objects is less than 1 Myr and similar to that of class II radio-emitting sources and to the YSO core population as a whole. A significant population of YSOs in dense cores have retained their circumstellar disks for a much shorter time than most T Tauri stars. This confirms the result of André et al. (1992) for the stronger radio sources and extends the phenomenon to include the weaker emitters. Radio surveys are an important complement to infrared and X-ray surveys in identifying this population of diskless YSOs.

We would like to thank University of Missouri-St. Louis undergraduates Tina Fanetti and Sandy Davis for assistance with the data reduction and analysis. We also thank Ken Ganga and Nancy Lieberman of IPAC for their assistance with the ISOCAM data reduction. Mike Ressler generously provided data on WL 20 in advance of publication. We gratefully acknowledge the support of JPL contract 961514 to the University of Missouri-St. Louis.

REFERENCES

Abergel, A., et al. 1996, A&A, 315, L329
Adams, F., Lada, C., & Shu, F. 1987, ApJ, 213, 788
André, P. 1994, in the Cold Universe, ed. T. Montmerle, C. Lada, I. Mirabel, & J. Trân Thanh Vân (Gif-sur-Yvette: Editions Frontières), 179
———. 1996, in ASP Conf. Ser. 93, Radio Emission from the Stars and the Sun, ed. A. R. Taylor & J. M. Paredes (San Francisco: ASP), 273
André, P., Deeney, B. D., Phillips, R. B., & Lestrade, J.-F. 1992, ApJ, 401, 667
André, P., Martin-Pintado, J., Depois, D., & Montmerle, T. 1990, A&A, 236, 180
André, P., & Montmerle, T. 1994, ApJ, 420, 837
André, P., Montmerle, T., & Feigelson, E. 1987, AJ, 93, 1182
Anglada, G. 1996, in ASP Conf. Ser. 93, Radio Emission from the Stars and the Sun, ed. A. R. Taylor & J. M. Paredes (San Francisco: ASP), 3
Barsony, M., Kenyon, S., Lada, E., & Teuben, P. 1997, ApJS, 112, 109
Bessell, M. S., & Brett, J. M. 1988, PASP, 100, 1134
Bontemps, S. 1996, Ph.D. thesis, Univ. Paris XI
Bontemps, S., & André, P. 1997, in Poster Proc. IAU Symp. 182, Low-Mass Star Formation: From Infall to Outflow, ed. F. Malbet & A. Castets (Paris: IAU), 63
Bontemps, S., André, P., Terebey, S., & Cabrit, S. 1996, A&A, 311, 858
Bontemps, S., et al. 2001, A&A, in press
Bouvier, J., & Appenzeller, I. 1992, A&AS, 92, 481
Casanova, S., Montmerle, T., Feigelson, E. D., & André, P. 1995, ApJ, 439, 752
Castelaz, M., Hackwell, J., Grasdalen, G., Gehrz, R., & Gullixson, G. 1985, ApJ, 290, 261
Chen, H., Myers, P., Ladd, E., & Wood, D. 1995, ApJ, 445, 377
D'Antona, F., & Mazzitelli, I. 1994, ApJS, 90, 467
———. 1997, Mem. Soc. Astron. Italiana, 68, 4
de Zeeuw, P. T., Hoogerwerf, R., de Bruijne, J. H. J., Brown, A. G. A., & Blaauw, A. 1999, AJ, 117, 354
Draine, B. T., & Lee, H. M. 1984, ApJ, 285, 89

Elias, J. H. 1978, ApJ, 224, 453
Feigelson, E. D., & Montmerle, T. 1985, ApJ, 289, L19
Grasdalen, G. L., Strom, K. M., & Strom, S. E. 1973, ApJ, 184, L53
Greene, T. P., & Lada, C. J. 1996, AJ, 112, 2184
———. 1997, AJ, 114, 2157
———. 2000, AJ, 120, 430
Greene, T. P., & Meyer, M. R. 1995, ApJ, 450, 233
Greene, T. P., Wilking, B., André, P., Young, E., & Lada, C. J. 1994, ApJ, 434, 614
Greene, T. P., & Young, E. T. 1992, ApJ, 395, 516
Grosso, N., Montmerle, T., Bontemps, S., André, P., & Feigelson, E. 2000, A&A, 359, 113
Kamata, Y., Koyama, K., Tsuboi, Y., & Yamauchi, S. 1997, PASJ, 49, 461
Kenyon, S., Lada, E., & Barsony, M. 1998, AJ, 115, 252
Kenyon, S. J., Whitney, B., Gomez, M., & Hartmann, L. 1993, ApJ, 414, 773
Lada, C. J. 1987, in Star Forming Regions, ed. M. Peimbert & J. Jugaku (Dordrecht: Kluwer), 1
Lada, C. J., & Adams, F. J. 1992, ApJ, 393, 278
Lada, C. J., & Wilking, B. A. 1984, ApJ, 287, 610
Leous, J. A., Feigelson, E. D., André, P., & Montmerle, T. 1991, ApJ, 379, 683
Loren, R. B., & Wootten, H. A. 1986, ApJ, 306, 142
Loren, R. B., Wootten, H. A., & Wilking, B. A. 1990, ApJ, 365, 269
Looney, L. W., Mundy, L. G., & Welch, W. J. 2000, ApJ, 529, 477
Luhman, K. L., & Rieke, G. H. 1999, ApJ, 525, 440
Lutz, D., et al. 1996, A&A, 315, L269
Meyer, M. R., Calvet, N., & Hillenbrand, L. A. 1997, AJ, 114, 288
Montmerle, T., Feigelson, E., Bouvier, J., & André, P. 1993, in Protostars & Planets III, ed. E. H. Levy & J. I. Lunine (Tucson: Univ. Arizona Press: Tucson), 689
Montmerle, T., Koch-Miramond, L., Falgarone, E., & Grindlay, J. E. 1983, ApJ, 269, 182
Motte, F., André, P., & Neri, R. 1998, A&A, 336, 150
Myers, P. C., & Ladd, E. F. 1993, ApJ, 413, L47
Palla, F., & Stahler, S. 1999, ApJ, 525, 772
Ressler, M. E., & Barsony, M. 2001, AJ, 121, 1098
Rieke, G. H., & Lebofsky, M. J. 1985, ApJ, 288, 618
Skrutskie, M., Dutkevitch, Strom, S., Edwards, S., & Strom, K. 1990, AJ, 99, 1187
Starck, J. L., Abergel, A., Aussel, A., Sauvage, M., Gaustad, R., Claret, A., Desert, X., Delattre, C., & Pantin, E. 1999, A&AS, 134, 135
Stine, P. C., Feigelson, E., André, P., & Montmerle, T. 1988, AJ, 96, 1394
Strom, K. M., Kepner, J., & Strom, S. E. 1995, ApJ, 438, 813
Strom, K., Strom, S., Edwards, S., Cabrit, S., & Skrutskie, M. 1989, AJ, 97, 1451
Struve, O., & Rudkjobing, M. 1949, ApJ, 109, 92
Tokunaga, A. T. 2000, in Astrophysical Quantities, ed. A. N. Cox (4th ed.; Dordrecht: Springer), 143
Vrba, F. J., Strom, S. E., Strom, K. M., & Grasdalen, G. L. 1975, ApJ, 197, 77
Walter, F., Brown, A., Mathieu, R., Myers, P., & Vrba, F. 1988, AJ, 96, 297
Wilking, B. A. 1991, in Low-Mass Star Formation in Southern Molecular Clouds, ed. Bo Reipurth (Garching: ESO), 159
Wilking, B. A., & Lada, C. J. 1983, ApJ, 274, 698
Wilking, B. A., Greene, T. P., & Meyer, M. R. 1999, AJ, 117, 469
Wilking, B. A., Lada, C. J., & Young, E. T. 1989, ApJ, 340, 823
Young, E., Lada, C. J., & Wilking, B. A. 1986, ApJ, 304, L45